Development of Mismatch Repair-Fluorescent Protein Fusion for Single Molecule Imaging

Undergraduate Research Thesis

Presented in Partial Fulfillment of the Requirements for graduation "with Honors Research

Distinction in Biology" in the undergraduate colleges of The Ohio State University

By

Joshua Mangels

The Ohio State University

April 2018

Project Advisor: Dr. Richard Fishel, Department of Cancer Biology and Genetics

Abstract:

DNA mismatch repair (MMR) is an essential process for maintaining genome integrity. Defective MMR can lead to the hereditary cancer predisposition Lynch Syndrome, as well as 10-40% of related cancers[1]. MMR removes a mismatched DNA nucleotide and replaces it with the correct one[2]. This process involves the formation of a cascade of highly conserved MMR protein complexes on DNA[3]. These conserved proteins include the MutS and MutL proteins in *Escherichia coli* and their homologs in other organisms[1]. Knowing how the MutS and MutL homolog complexes interact with DNA and each other is crucial for understanding MMR. A powerful method for studying such interactions is single-molecule total internal reflection fluorescence (smTIRF) microscopy. To visualize MMR using smTIRF, individual proteins must be labeled with a fluorophore. Engineered fluorescent proteins that contain specific excitation and emission properties have been used in smTIRF. This project sought to establish useful fluorescent proteins to study MMR *in vivo* by identifying the far-red fluorescence spectrum of the fluorescent protein miRFP670 and constructing two fluorescent protein fusions: MutS-mTagBFP and MutS-mEos3.2. In preliminary studies, the emission spectrum of purified miRFP670 was obtained via spectrofluorimetry. The expression of MutS-mTagBFP was optimized and a purification protocol developed. MutS-mEos3.2, however, appeared to inhibit normal MutS function and was not pursued further.

Introduction

Cancer is one of the deadliest diseases that affects humans[4]. Some fundamental causes of cancer include exposure to carcinogens and genetic predisposition that ultimately triggers cellular

tumorigenesis[4]. One of the most common genetic predispositions to cancer is Lynch Syndrome (LS)[1]. LS is caused by faulty DNA mismatch repair (MMR), potentially leading to a range of cancers—including colorectal, endometrial, and ovarian cancer[1]. Defective MMR can result from a loss of function mutation in any one of the core MMR proteins, including MutS or MutL in *Escherichia coli*, or the MutS Homolog 2 (MSH2), MutS Homolog 6 (MSH6), MutL Homolog 1 (MLH1), or the MutL homolog originally designated as Postmeiotic Segregation 2 (PMS2) in humans[1].

MMR is a critical cellular process required to maintain genome stability by reducing the number of DNA polymerase misincorporation errors during replication[2]. MMR involves the recognition and excision of a mismatched nucleotide followed by resynthesis with the correct nucleotide[2]. In *E coli*, this process is executed by a cascade of proteins including MutS, MutL, MutH, and UvrD. Strand discrimination in *E. coli* MMR is based on a temporary lack of DNA methylation at GATC sites in the nascent strand containing the misincorporation error[5]. These sites are methylated by Dam methylase after replication, however methylation does not occur immediately[5]. This lag allows the MMR machinery to recognize and replace the incorrect nucleotide within a mismatch before the newly-replicated strand is methylated.

MutS functions as a homodimer and forms a searching clamp that transiently binds DNA and slides along the helix to identify mismatched nucleotides. Once a mismatch is detected, MutS binds ATP and undergoes a conformational change into a significantly more stable sliding clamp[3]. The ATP-bound MutS recruits a MutL homodimer that also binds ATP, forming a second sliding clamp[3]. This MutS-MutL complex recruits MutH to form a search complex on the DNA to find a hemimethylated GATC site. MutH then nicks the DNA on the unmethylated error-containing strand[2]. The MutS-MutL complex or MutL alone recruits the UvrD DNA helicase, which acts

with a single-stranded DNA exonuclease to excise the nascent, mismatch-containing daughter strand just beyond the mismatch[2]. The remaining DNA gap is resynthesized by the cellular replicative DNA polymerase independent of the core MMR components[3]. The MMR pathway also acts as a damage sensor in higher eukaryotes to induce apoptosis and prevent tumorigenesis when DNA damage is too extensive to repair[6].

Understanding MMR in *E. coli* can be quite useful as humans have homologous proteins that repair polymerase errors. One way to study MMR is by single molecule total internal reflection fluorescence (smTIRF) microscopy using fluorescent proteins. This process involves fusion of an MMR protein and a fluorescent protein, expressed as a single transcript. Excitation of the fluorescent protein domain will cause a characteristic fluorescent emission that can be detected to visualize the fusion protein. Single molecule imaging techniques can track such fusion proteins on mismatched DNA to observe diffusion rates, lifetime, and complex formation.

The use of fluorescent resonance energy transfer (FRET) can improve the resolution of these studies to nanometer distances. FRET occurs when one fluorophore, a FRET donor, is excited and emits electromagnetic radiation (EMR) of a characteristic wavelength. If this is in the excitation range of a nearby fluorophore, a FRET acceptor, then energy can be transmitted to the second fluorophore and it may be excited. This second fluorophore, if excited, will emit EMR of a different wavelength, allowing visualization of the acceptor[7]. However, this technique only works if the two fluorophores are in extremely close proximity to each other, 1-10 nm[7]. Therefore, this is an excellent method to determine molecular proximity and interaction. The fluorophore constructs produced in this project were chosen as potential FRET pairs to determine the proximity of MutS to other MMR fusion proteins. These methods will be utilized to improve our understanding of MMR.

A deeper understanding of the functionality of MMR proteins can have implications in the diagnosis of LS. If a mutation is present in an MMR gene, how does one know if it causes the loss of function of that protein as in LS? A greater knowledge of how these proteins work could reveal what causes them to fail, such as mutation in a certain domain or sequence of the protein. If mutations that disable a MMR protein are identified, then a genetic screen revealing that mutation can be indicative of LS. While this project involves *E. coli* MMR proteins, due to the conserved nature of these proteins among organisms the effects of these mutations may be similar in human MMR proteins.

In this project, two experimental objectives were accomplished. The first was expression, purification, and verification of the emission spectrum of the far-red fluorescent protein miRFP670. The second was construction of two fluorescent protein fusion constructs: MutS-mTagBFP and MutS-mEos3.2. MutS-mTagBFP was purified. However, after construction of the MutS-mEos.2 fusion gene, it did not display the MutS phenotype and was not purified.

Methods

miRFP670

Originally, the protein iRFP670 was going to be used in this project. However, it was later discovered that iRFP670 is a dimer and therefore naturally oligomerizes. This potential oligomerization could disrupt MMR protein function of tagged protein constructs in single molecule visualization experiments. Therefore, a monomeric isoform, miRFP670, was obtained to complete this project begun with iRFP670.

The iRFP670 gene was inserted into the expression vector pET-29a, a plasmid containing the lactose promoter, operator, and repressor. Using polymerase chain reactions (PCR), iRFP670

was amplified and a His-tag–a chain of six histidine codons—was added to the 3' end of the gene (C-terminus of the protein). Restriction endonuclease digestion and ligation with pET-29a completed the insertion. This plasmid, pET-29a-iRFP670, was transformed into XL-10 Gold cells to produce copies. The plasmid was cut with a single site restriction endonuclease and examined on an agarose gel to ensure that iRFP670 was inserted into the plasmid by examining its restriction enzyme pattern. It was completely sequenced as confirmation.

It was at this point when we discovered that iRFP670 was a dimer. A plasmid containing miRFP670 with an N-terminal His-tag was obtained and used for expression. This plasmid was transformed into BL21-(DE3)PlyS *E. coli* cells to express miRFP670. These cells were grown at varying temperature and concentration of the Lac-promoter inducer Isopropyl β-D-1-thiogalactopyranoside (IPTG) until sufficient soluble protein for purification was obtained. A different cell line, BL21-AI (arabinose inducible) *E. coli* cells, was also used—0.2% arabinose was included in induction when using this cell line. Soluble protein quantity was qualitatively determined by lysing cells and denaturing protein with sodium dodecyl sulfate, followed by peptide separation using polyacrylamide gel electrophoresis (PAGE).

Once sufficient soluble protein was obtained, cells were grown in one liter of LB (Luria Broth) media overnight and pelleted. miRFP670 was purified from these pellets via fast protein liquid chromatography (FPLC). The cells were lysed by freeze thawing cycles and sonication, followed by ultracentrifugation at 41,000 revolutions per minute for one hour. Soluble protein remained in the supernatant and was isolated and purified with a Nickel-NTA column. His-tagged proteins bind to this column. A gradient of imidazole (20-200 mM) was used to compete with the His-tag and elute miRFP670. The fractions containing protein were determined as a peak of protein-dependent 280 nm absorbance during elution. Peptides from these fractions were

separated on a PAGE gel to determine identity and purity of the protein. Highly enriched fractions were dialyzed in a buffer of 25 mM HEPES, 150 mM NaCl, 1 mM DTT, 0.1 mM EDTA, and 20% glycerol and stored at -80° C. The concentration was determined using the Beer-Lambert Law:

Protein concentration (M) = (Absorbance at 280 nm)/(ε_{280}=Molar extinction coefficient at 280 nm ($M^{-1}cm^{-1}$))*(cell pathlength (cm))

The molar extinction coefficients were determined using the protein sequence[8]. The pathlength was 0.1 cm for the instrument that was used to determine the absorbance.

This purified protein was then used in spectrofluorimeter experiments. A spectrofluorimeter excites a fluorophore at a defined wavelength and measures its emission spectrum. The optimal excitation wavelength for miRFP670, as shown in the literature, is 642 nm with the peak emission wavelength at 670 nm[9]. However, due to limitations of the laboratory's spectrofluorimeter, the emission wavelength must start at least 10 nm above the excitation wavelength. Thus, a full spectrum cannot be obtained using an excitation of 642 nm as the emission spectrum would be incomplete since it would begin at 652 nm. Therefore, the protein was excited at 600 nm to ensure a more complete emission spectrum.

MutS-mTagBFP/MutS-mEos3.2

Two MutS derivates were constructed with a fluorescent protein fused to the C-terminus and a C-terminal His-tag. The MutS gene and fluorescent protein genes (mTagBFP and mEos3.2) were amplified by PCR. The fluorescent protein contained the His-tag on the 3' end (C-terminal). The primers contained identical sequences on the 3' (C-terminal) end of the MutS gene and the 5' (N-terminal) end of the fluorescent protein gene. The identical sequence, or fusion sequence, from the MutS and fluorescent protein fragments were annealed in an overlap PCR. No primers were added to allow the overlapping sequences on each gene to anneal and be extended by PCR, linking the two genes into one double stranded fragment. After three cycles, primers from the ends of the

fusion strand were added to amplify the entire fragment. Insertion into pET-29a, sequencing, and optimization of expression of MutS-mTagBFP were performed as described for iRFP670/miRFP670.

MutS-mTagBFP was purified. The first attempt used a Ni-NTA column. However, no protein bound to the nickel resin. We hypothesize that the lack of a peptide linker region between the protein and the His-tag may have caused the His-tag to be inaccessible to the column. Therefore, Heparin (ion exchanger), Gel Filtration (size exclusion), and MonoQ (ion exchanger) columns were used, in that order, to purify the protein. In the ion exchange columns, the protein binds to the column and is then eluted by NaCl. The gel filtration column separates components based on shape and molecular weight, where the larger proteins migrate through the column faster. The peptides obtained from these columns were examined on PAGE gels to determine purity and identity. Highly enriched protein was dialyzed and the concentration determined as described for miRFP670.

Upon completion of the MutS-mEos3.2 construct, sequencing revealed a nonsense mutation at codon 432. This was reverted to the wild type amino acid by site directed mutagenesis[10]. Primers of 25 nucleotides complementary to the regions adjacent to the mutation and containing the reversion mutation were used to perform PCR. The product was treated with the endonuclease DpnI to degrade non-mutated bacterial DNA. DpnI digests methylated DNA, and because *E. coli* DNA is methylated it is degraded. The newly synthesized DNA—unmethylated because it was obtained from PCR and not from *E. coli*—containing the reversion mutation is not degraded. The plasmid was resequenced to confirm the reversion then transformed into BL21-AI cells for expression.

Upon expression, no MutS-mEos3.2 protein was observed. A complementation assay was performed to determine the functionality of MutS-mEos3.2. Since MutS is a major protein of the MMR pathway, it is important in maintaining genome integrity[2]. If it is mutated or absent, mutations will accumulate in the genome at a faster rate as a result of defective MMR. This will eventually lead to mutations in the ribosome that may be detected as resistance to the antibiotic rifampicin[11]. The MutS-mEos3.2 construct was transformed into MutS-deficient (ΔMutS) cells lacking the MutS gene. If addition of MutS-mEos3.2 to ΔMutS cells complements and rescues the MutS phenotype, then the cells will not develop rifampicin resistance and display few, if any rifampicin-resistant colonies. If the addition of MutS-mEos3.2 does not complement and fails to rescue the MutS phenotype, then the cells will display many rifampicin-resistant colonies, indicating the MutS fusion is non-functional.

Results

miRFP670

The optimization of expression of miRFP670 in BL21-AI cells revealed that sufficient soluble protein was obtained with growth at 25° C, 1 mM IPTG, and 0.2% arabinose overnight (Figure 1). Cells were grown under these conditions and pellets were made for purification. The molecular weight of miRFP670 is 35.9 kDa. The protein was injected into a Nickel-NTA column attached to an FPLC. The His-tag fused to the N-terminus of miRFP670 bound the nickel resin. Protein was then eluted with a 20-200 mM imidazole gradient to compete with the His-tag (Figure 2). This resulted in highly enriched, concentrated protein (13.30 μM).
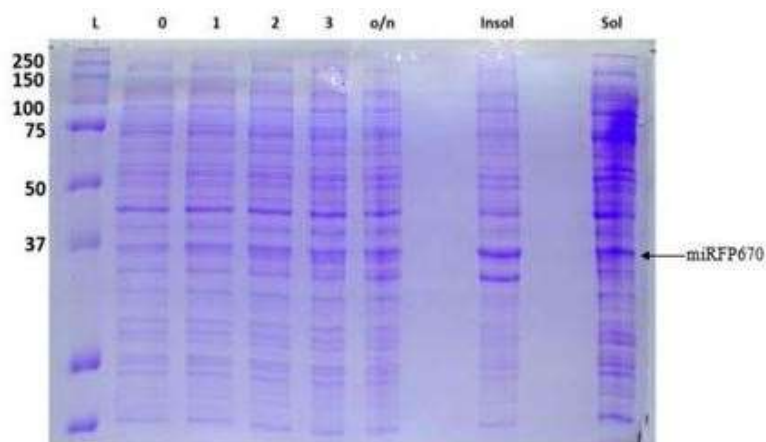
Figure 1: miRFP670 Expression at 25° C, 1 mM IPTG, 0.2% Arabinose; L=molecular weight ladder (in kDa), #=hour after induction, o/n=overnight, Insol=insoluble protein, Sol=soluble protein
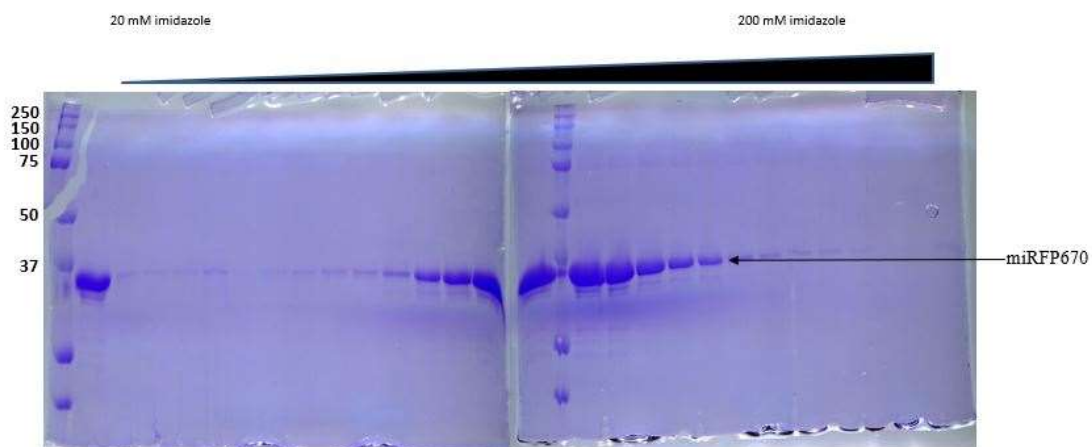

Figure 2: PAGE Gel of Purification of miRFP670 with a Ni-NTA Column

This purified protein was used in spectrofluorimeter studies to confirm peak emission before use in single molecule experiments. The emission spectrum excited at 600 nm is shown in Figure 3, with a peak emission at 670 nm. However, there is a significant emission at the beginning of the spectrum that was a result of the laser used to excite the fluorescent protein (600 nm) (Figure 3a). To ensure that the spectrum was a result of miRFP670 emission, we employed a Chroma filter that blocked the 600 nm laser and only allowed 665-705 nm emission. This range includes the peak emission of miRFP670[9]. This clarified spectrum is shown in Figure 3b, showing that the 670 nm peak is clearly a result of miRFP670.
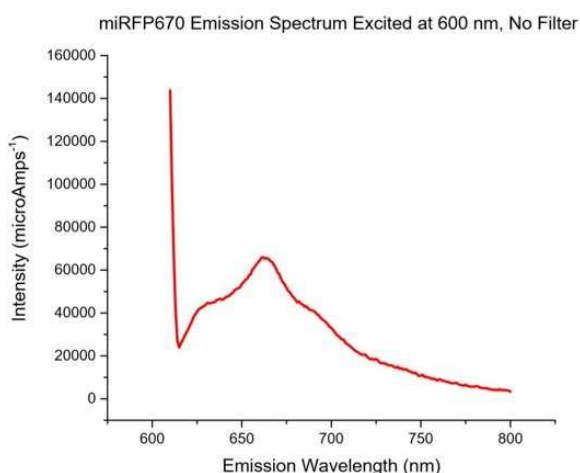
Figure 3a: miRFP670 Emission Spectrum Excited at 600 nm with no filter
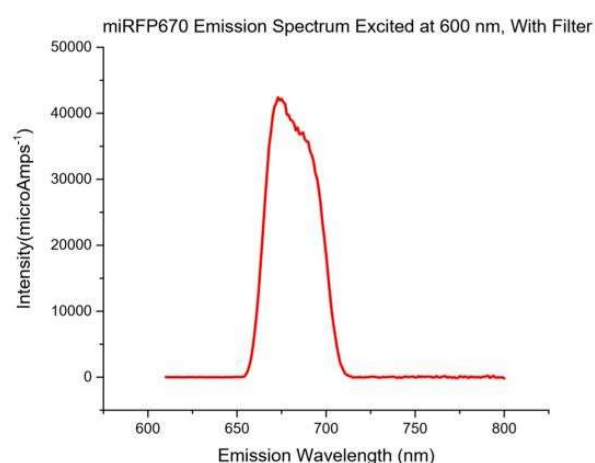
Figure 3b: miRFP670 Emission Spectrum Excited at 600 nm with filter

The peak emission of miRFP670 should transverse a band-pass filter used in the laboratory's cellular single molecule imaging system. This is a different filter than the one used to clarify the emission spectrum in Figure 3b. Figure 4 shows the spectrum of the band-pass filter in the cellular single molecule imaging instrument is approximately 665-740 nm[12]. The emission spectrum of miRFP670 suggests that it will traverse this band-pass filter allowing visualization. This is an important observation for future laboratory single molecule studies.
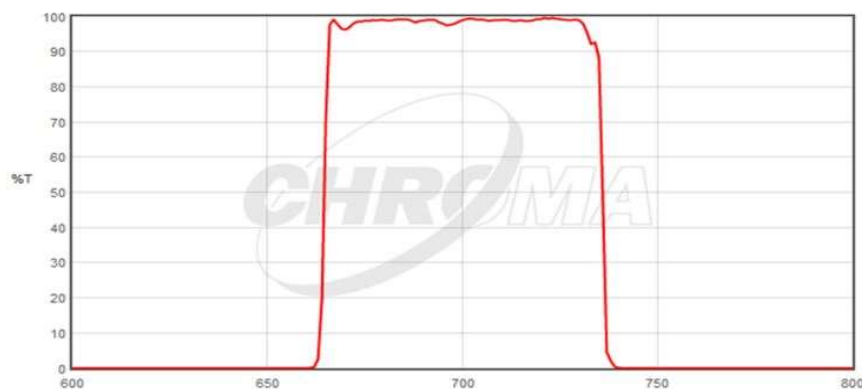
Figure 4: Light able to pass through the band-pass filter[12]

Another aim of purifying miRFP670 was to establish whether it might be utilized as a FRET pair with mEos3.2 as the donor. Based on the spectra, mEos3.2 excited with a 532 nm laser emits in the 600-630 nm range [13] (Figure 5), suggesting that it should excite miRFP670. We conclude that mEos3.2 should be able to excite miRFP670 if they are close enough for FRET to occur.
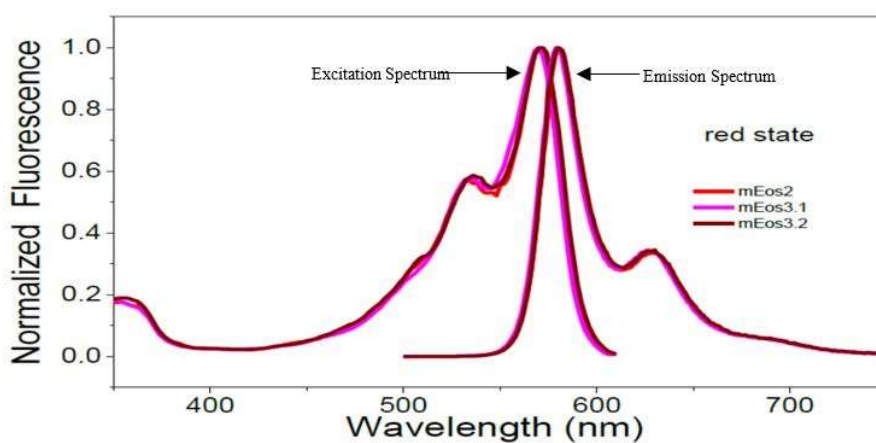

Figure 5: Excitation and Emission Spectra of mEos3.2[13]

MutS-mTagBFP

The optimal expression for the MutS-mTagBFP construct was achieved in BL21-AI cells. The cells were grown to OD=0.3 at 37 ° C, cooled to 16 ° C for 30 minutes, and then induced with 0.5 mM IPTG and 0.2% arabinose (Figure 6). The molecular weight of this protein is 129.5 kDa,
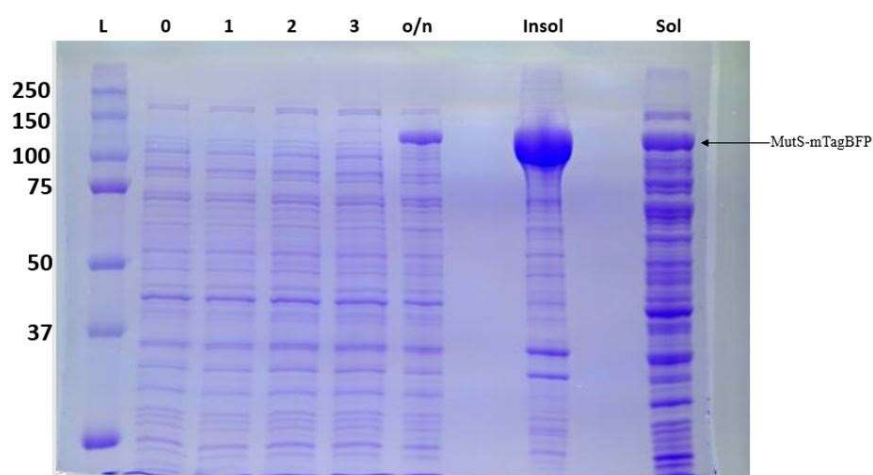

Figure 6: PAGE Gel of Optimal Expression of MutS-mTagBFP

thus it will appear between the 100 kDa and 150 kDa markers on PAGE gels. Soluble protein was injected into a Ni-NTA column, however it did not bind the column (last 6 lanes of Figure 7). The His-tag was likely inaccessible and unable to bind the Nickel resin, therefore it could not be
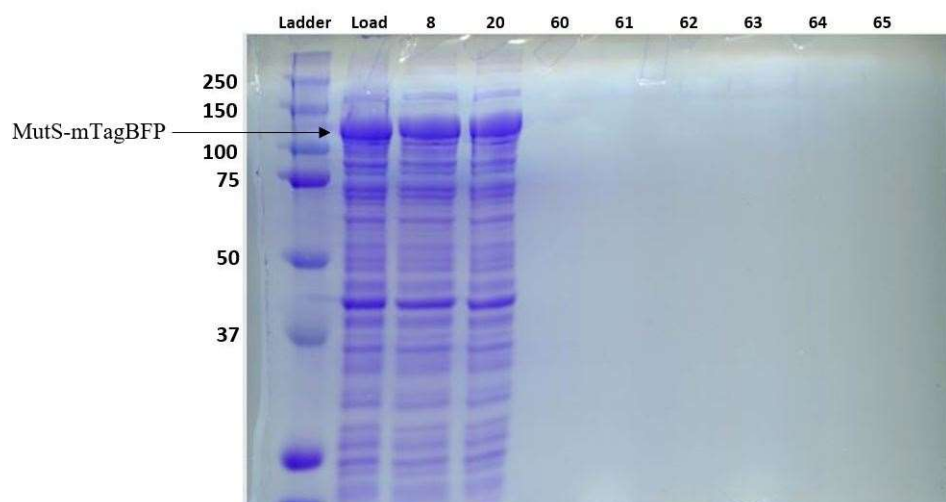

Figure 7: PAGE Gel of MutS-mTagBFP Purified with a Ni-NTA Column

purified using this affinity tag system. The chromatograph at 280 nm absorption is shown (Figure 8). The fractions correlating to 280 nm absorbance peaks were analyzed on PAGE gels. Figure 8

shows only one 280 nm peak where protein may have eluted from the column. However, the PAGE gel (Figure 7) shows no protein in these fractions.
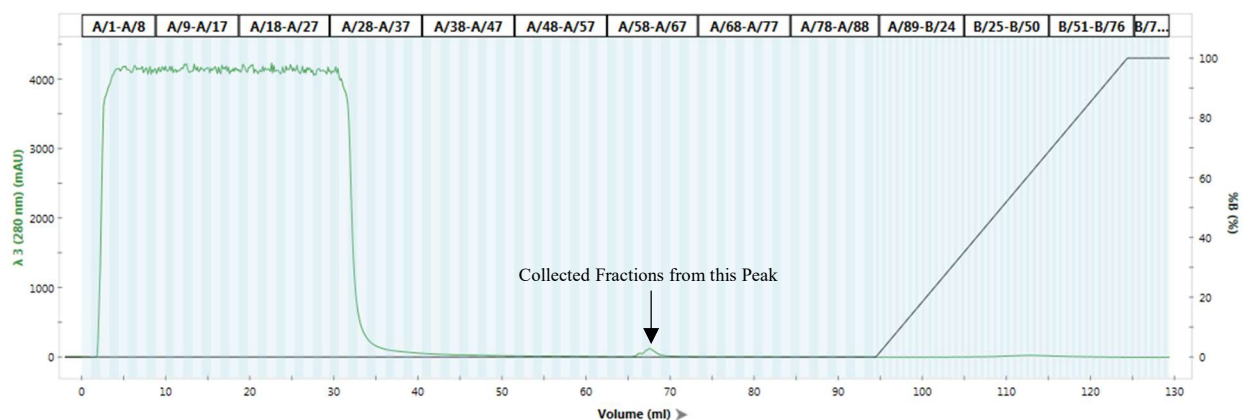

Figure 8: Chromatograph of MutS-mTagBFP Ni-NTA Purification, Green line denotes 280 nm absorbance, Black line denotes salt concentration

MutS-mTagBFP was purified from another induced cell pellet using a Heparin column—ion exchanger—(Figure 9), Superdex 200 gel filtration column—size exclusion column—(Figure 11), and a MonoQ Column—ion exchanger—(Figure 13). The chromatographs at 280 nm absorption are shown after each gel (Figures 10, 12, 14). After the MonoQ column, the protein had few contaminants and a concentration of 1.38 µM. Despite these protein contaminants, it was sufficiently pure to conduct preliminary biochemical experiments.
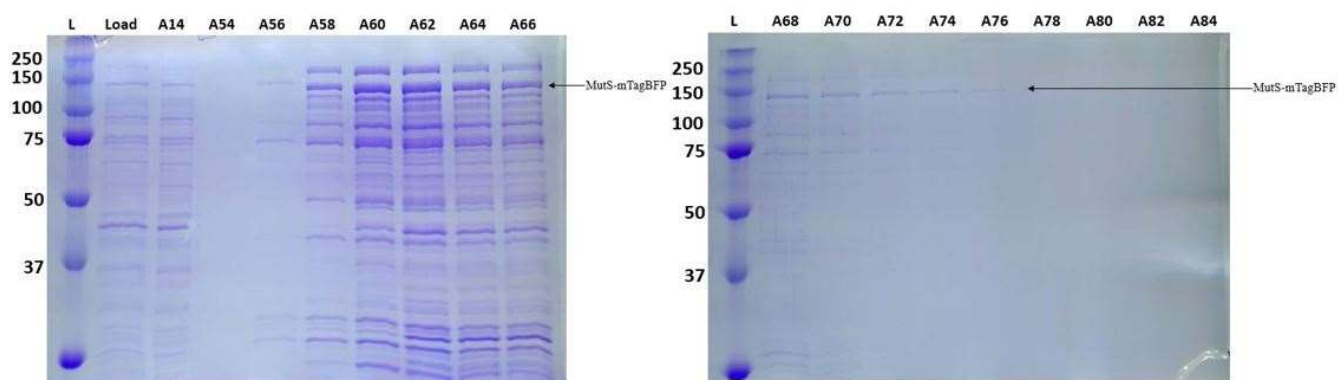

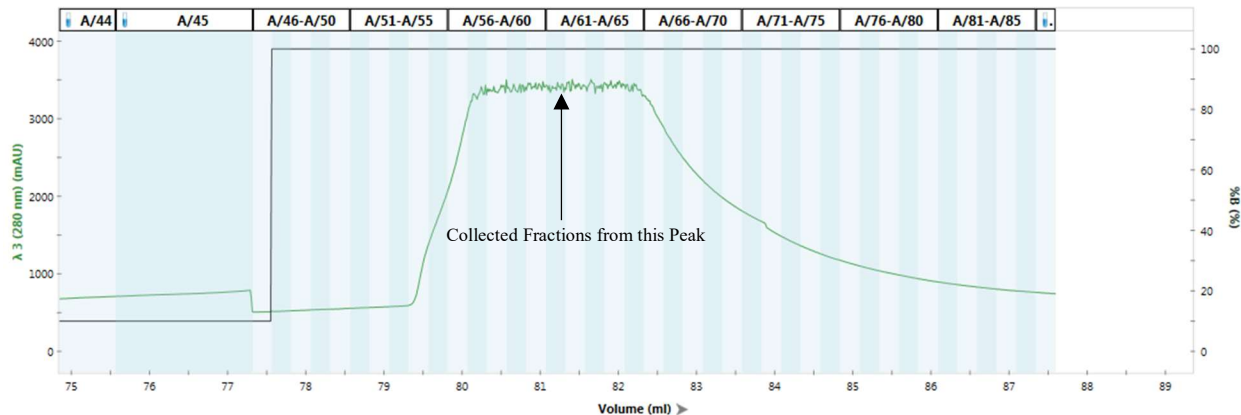*Figure 9: PAGE Gel of MutS-mTagBFP Purified with Heparin Column*

Figure 10: Chromatograph of MutS-mTagBFP Heparin Column Purification, Green line denotes 280 nm absorbance, Black line denotes salt concentration
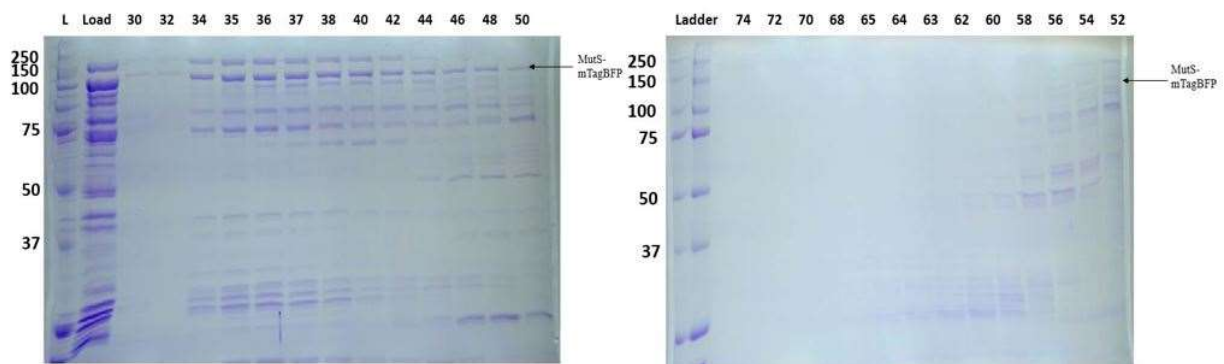

Figure 11: PAGE Gels of MutS-mTagBFP purified with Gel Filtration Column after purification with a Heparin Column
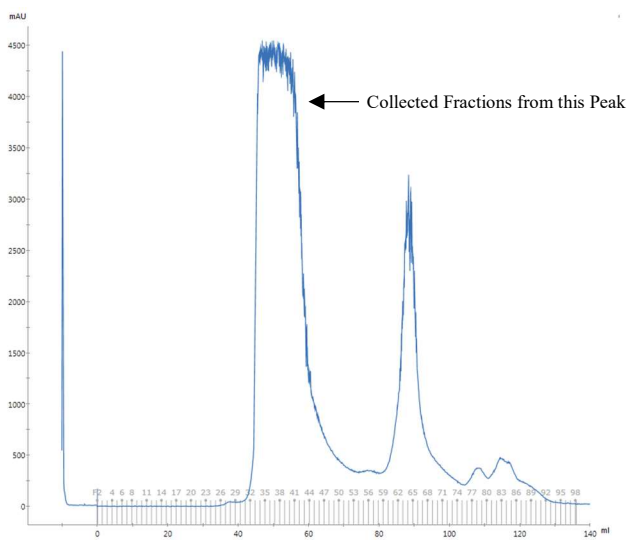

Figure 12: Chromatograph of MutS-mTagBFP Gel Filtration Column Purification, 280 nm absorbance
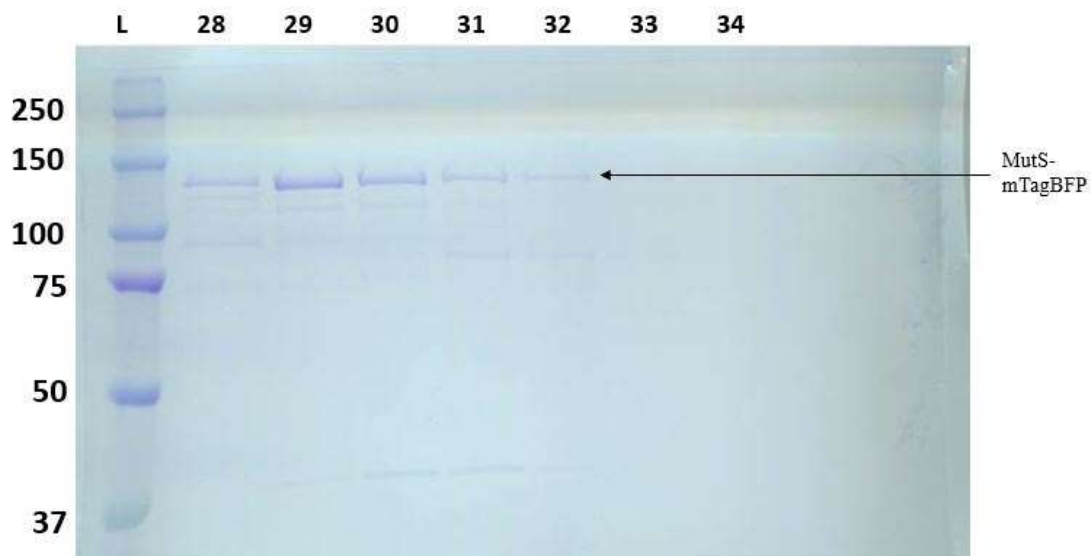
Figure 13: PAGE Gel of MutS-mTagBFP Purified with MonoQ Column after Purification with Heparin and Gel Filtration Columns
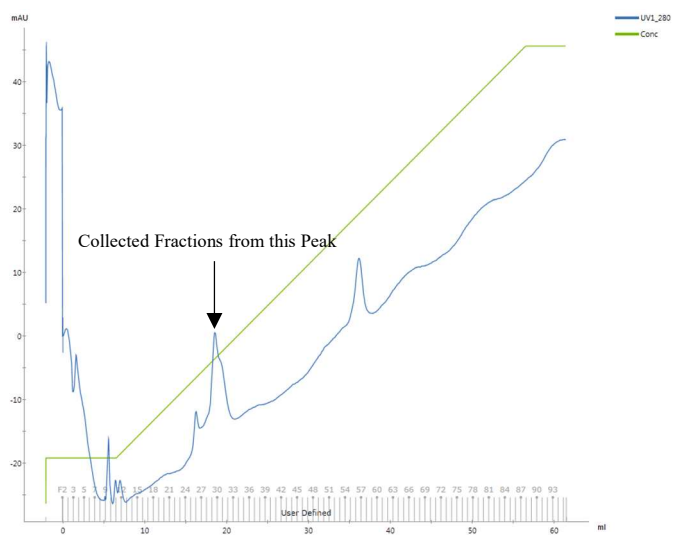

Figure 14: Chromatograph of MutS-mTagBFP MonoQ Column Purification, Blue line denotes 280 nm absorbance, Green line denotes salt concentration

These preliminary biochemical studies included tests performed by a graduate student, Brooke M Britton, in the laboratory to determine DNA binding and dissociation of the MutS-mTagBFP protein. The kinetics of enriched MutS-mTagBFP binding to mismatched DNA and

dissociation upon addition of ATP were consistent with wild type MutS. She also confirmed clamp formation of MutS-mTagBFP was similar to untagged MutS. These experiments show that this construct, with the addition of the fluorescent tag, behaves like wild type MutS *in vitro*.

Additionally, Ms. Britton performed a complementation assay to determine if the MutS-mTagBFP protein functioned properly *in vivo*. The gene was transformed into ΔMutS cells that are deficient in the MutS protein, and therefore MMR-defective. The MutS-mTagBFP construct complemented the MutS MMR deficiency as is demonstrated by significantly reduced formation of rifampicin-resistant colonies as compared to ΔMutS (Figure 15).
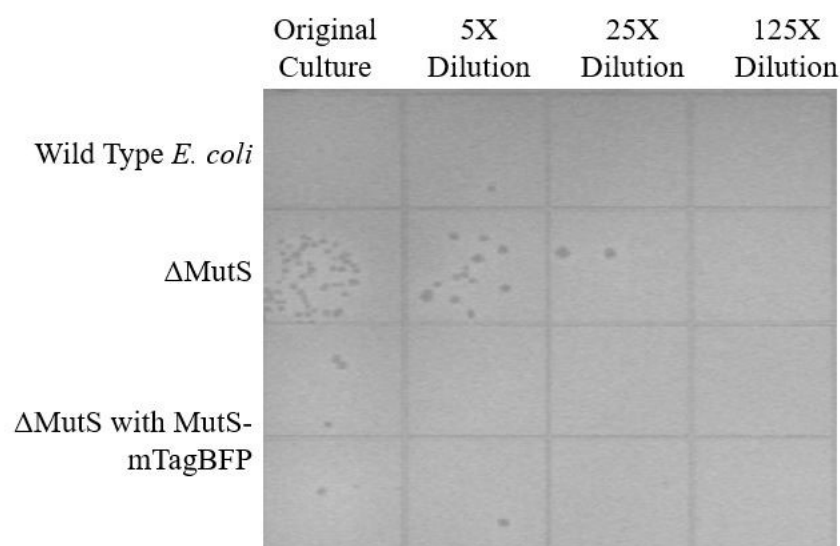

Figure 15: Complementation Assay of MutS-mEos3.2, Dilution=100 µL of culture in 400 µL of 0.85% Saline, Performed by Brooke M Britton

MutS-mEos3.2

Upon sequencing of the MutS-mEos3.2 construct, it was discovered that a nonsense mutation occurred at the 432nd amino acid, a glutamate. This was reverted via site directed mutagenesis[10] and confirmed by resequencing. Upon expression of this fusion, no protein at the corresponding molecular weight of 122.02 kDa was observed. Therefore, a complementation

assay was performed to determine the functionality of the MutS-mEos3.2 protein. The MutS-mEos3.2 construct did not complement the MutS phenotype in the ΔMutS cell line. This is shown by the formation of many rifampicin-resistant colonies (Figure 16). A ΔMutL cell line was used as a control. The wild type *E. coli* appeared to display background growth that was absent in lower concentrations. We regard it likely that the volume of cells interfered with rifampicin selection. This also appeared to occur in high concentrations of ΔMutL. In contrast, the ΔMutS strain showed clear rifampicin-resistant colonies that displayed dilution dependence. ΔMutS cells containing MutS-mEos3.2 also developed rifampicin-resistant colonies, strongly suggesting that the plasmid containing this protein does not complement the wild type activity. It is unclear whether this is a result of the mEos3.2 tag or whether the protein is just not expressed appropriately.
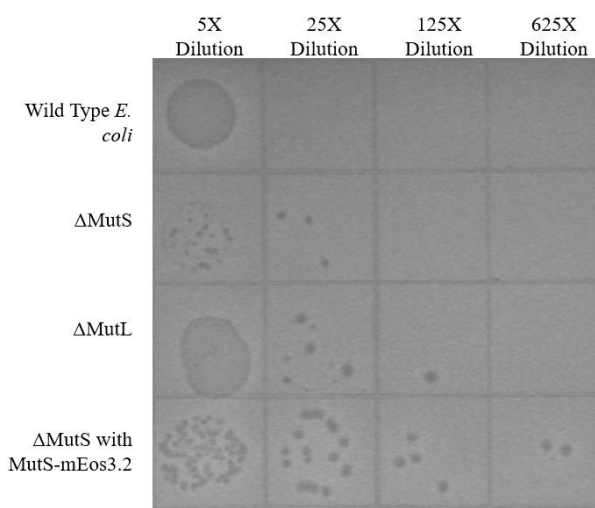

Figure 16: Complementation Assay of MutS-mEos3.2, Dilution=100 μL of culture in 400 μL of 0.85% Saline

Beyond the fact that MutS-mEos3.2 did not complement MutS function, it seems to have acted as a mutator due to the formation of many more rifampicin-resistant colonies as compared to ΔMutS. Given this point and the failure of the protein expression, there likely is a variable involved somewhere in the expression process that would be worth investigating in future studies.

Discussion/conclusion

This thesis demonstrates that the peak emission of miRFP670 is 670 nm. This is significant as the emission from this excited fluorescent protein will be able to traverse a band-pass filter in experiments utilizing the laboratory's cellular single molecule imaging instrument. Using a quadview, four band-pass filters can be arranged, with each permeable to only a defined range of emission unique to each filter. This system allows visualization of up to four different fluorophores. Thus, four fluorescent proteins can be included in the system with each one viewed separately and later merged to determine co-localization. This instrument is capable of monitoring the interaction of up to four different proteins during MMR. The work in this project suggests miRFP670 can be fused to any MMR protein and used in this system, since it emits light capable of passing through one of these band-pass filters. Previous work has suggested that the MutS-mTagBFP construct may also be used in these experiments. However, the emission spectrum was not obtained.

Based on the results of this project, miRFP670 and mEos3.2 should be a compatible FRET pair with mEos3.2 as the donor and miRFP670 as the acceptor; however, this will need to be tested empirically for confirmation. If they are a compatible pair, FRET may occur when they are tagged to MMR proteins. If it occurs, then it highly suggests an interaction between the MMR proteins. This will occur when mEos3.2 is excited by a laser that will not excite miRFP670 and 670 nm light is emitted. This method is an improvement upon the laboratory's current method of co-localization. Co-localization with fluorescent proteins from a different frame of the quadview, containing the band-pass filters, is currently used to determine interaction of MMR proteins. However, the resolution is diffraction limited, limited by the wavelength of light used[14]. The resolution is approximately 300 nm. Therefore, when molecules co-localize they could be

interacting or they could be up to 300 nm apart. Utilizing FRET, interaction can be calibrated to within 10 nm. Increasing the resolution will provide information with more precision, such as the interaction of two proteins with each other and for how long it occurs.

Only fusion constructs for the MMR protein MutS were constructed and purified in this project. However, this can be done with additional MMR proteins to study further the function and interaction of these proteins. More fusion protein constructs, with previously studied fluorescent proteins, will be created including MutL-PSmOrange and ß-Clamp-miRFP670.

A better understanding of MMR protein complexes can lead to a more complete appreciation of their role in LS—possibly leading to better diagnostic tools. For example, the study of the effects on single amino acid changes or other alterations of MMR proteins in *E. coli* can reveal which mutations lead to defective MMR and which do not. Due to the homology of human and *E. coli* MMR proteins, this knowledge could potentially be extrapolated in order to determine what mutations cause loss of function in human MMR proteins and help diagnose LS.

Citations:

1: Lynch, H.T., Snyder, C.L., Shaw, T.G., Heinen, C.D. and Hitchins, M.P. (2015) Milestones of Lynch syndrome: 1895-2015. *Nat Rev Cancer*, 15, 181-194.

2: Fishel, R. (2015) Mismatch Repair. *J. Biol. Chem.*, 290 (44), 26395-26404.

3: Liu, J., Hanne, J., Britton, B.M., Bennett, J., Kim, D, Lee, J-B., and Fishel, R. (2016) Cascading MutS and MutL sliding clamps control DNA diffusion to activate mismatch repair. *Nature*, 539, 583-587.

4: Hanahan, D. and Weinberg R. A. (2011) Hallmarks of Cancer: The Next Generation. *Cell*. 144(5), 646-674.

5: Marinus, M. G. and Løbner-Olesen. A. (2014) DNA Methylation. *EcoSal Plus 2014.* doi:10.1128/ecosalplus.ESP-0003-2013

6: Wang, J. Y, and Edelmann, W. (2006) Mismatch repair proteins as sensors of alkylation DNA damage. *Cancer Cell*. 9, 417-418

7: Sekar, R.B. and Periasamy, A. (2003) Fluorescence resonance energy transfer (FRET) microscopy imaging of live cell protein localizations. *J. Cell Biol.*, 160 (5): 629–633.

8: Grimsley, G.R. and Pace, C. N. (2003) Spectrophotometric Determination of Protein Concentration. *Curr Protoc Protein Sci.* 33(1): 3.1.1-3.1.9.

9: Shcherbakova, D. M., Baloban, M., Emelyanov, A.V., Brenowitz, M., Guo, P., and Verkhusha, V.V. (2016) Bright monomeric near-infrared fluoresecent proteins as tags and biosensors for multiscale imaging. *Nature Communications*, 7, 12405.

10: Weiner, MP, Costa, GL, Schoettlin W, Cline J, Mathur E, Bauer, JC. (1994) Site-directed mutagenesis of double-stranded DNA by the polymerase chain reaction. *Gene*, 151, 119-123.

11: Lea, D.E., and Coulson C.A. (1949) The distribution of the numbers of mutants in bacterial populations. *J Genet*. 49(3):264-285.

12: Chroma. c2018. Bellows Falls, (VT). Chroma Technology Corporation; [accessed 2018 March 31]. http://www.scientificstyleandformat.org/Tools/SSF-Citation-Quick-Guide.html

13: Zhang, M., Chang, H., Zhang, Y., Yu, J., Wu, L., Ji, W., Chen, J., Liu, B., Lu, J., Liu, Y., Zhang, J., Xu, P., and Xu, T. (2012) Rational design of true monomeric and bright photoactivatable fluorescent proteins. *Nature Methods*. 9, 727-729

14: Murphy, D.B., and Davidson, M.W. (2012) Fundamentals of light microscopy and electronic imaging. *Wiley-Blackwell*, 2.